Breakdown of classical bunch length and energy spread formula in a quasi-isochronous electron storage ring

X. J. Deng,[1,*] A. W. Chao,[2,3] J. Feikes,[4,†] A. Hoehl,[5] W. H. Huang,[1] R. Klein,[5,‡] A. Kruschinski,[4] J. Li,[4] M. Ries,[4,§] and C. X. Tang[1]

[1]*Department of Engineering Physics, Tsinghua University, Beijing 100084, China*
[2]*Institute for Advanced Study, Tsinghua University, Beijing 100084, China*
[3]*Stanford University, Stanford, California 94309, USA*
[4]*Helmholtz-Zentrum Berlin (HZB), Albert-Einstein-Straße 15, 12489 Berlin, Germany*
[5]*Physikalisch-Technische Bundesanstalt (PTB), Abbestraße 2-12, 10587 Berlin, Germany*

(Received 21 December 2022; accepted 17 April 2023; published 5 May 2023)

Originating from the stochastic nature of the photon emission process, the longitudinal coordinates of electrons diffuse even if the global phase slippage of a storage ring is zero, as we cannot zero all the local phase slippages simultaneously. This quantum diffusion is viewed as the most fundamental effect limiting the lowest bunch length realizable in an electron storage ring from single-particle dynamics perspective. Energy spread diverges when bunch length is pushed to the limit given by this diffusion. Here we report the first experimental evidence supporting the existence of this effect. The measurements confirm the breakdown of the classical formula of bunch length and energy spread in an electron storage ring with globally small and locally large phase slippage.

DOI: 10.1103/PhysRevAccelBeams.26.054001

I. INTRODUCTION

Short electron bunches or microbunches are desired in synchrotron radiation sources to produce ultrashort radiation pulses for ultrafast science investigations. Short electron bunches also enable high-power high-flux coherent radiation generation, which could provide new opportunities for research like high-resolution angle-resolved photoemission spectroscopy and industry applications like extreme ultraviolet lithography. To satisfy the ever-increasing demand of science and industry on advanced light sources, accelerator scientists keep inventing and developing new scenarios and technologies. For example, a storage ring–based novel light source mechanism called steady-state microbunching (SSMB), which promises high-average-power narrow-band coherent radiation with wavelengths ranging from THz to soft x ray, is being actively studied with encouraging progress being achieved [1–21], in particular, the recent success of the SSMB proof-of-principle experiment [22].

To obtain short bunches in an electron storage ring, a well-known method is the implementation of a quasi-isochronous magnetic lattice, where

$$\eta = \frac{\Delta T/T_0}{\Delta E/E_0} = \frac{1}{C_0}\oint\left(\frac{D_x(s)}{\rho(s)} - \frac{1}{\gamma^2}\right)ds, \tag{1}$$

the phase slippage factor of the ring which quantifies the energy dependence of particle's revolution time is very small. In the definition of η, T_0 is the revolution period and $E_0 = \gamma m_e c^2$ is the energy of the reference particle, m_e is the electron rest mass, γ is the Lorentz factor, C_0 is the circumference of the ring, D_x is the horizontal dispersion, ρ is the bending radius of the trajectory, and s is the path length along the reference orbit. The reason behind this approach is the classical "zero-current" bunch length scaling law $\sigma_z \propto \sqrt{|\eta|}$, given by Sands [23]. However, from single-particle dynamics perspective, there is a fundamental effect limiting the lowest bunch length realizable in an electron storage ring. It originates from the stochasticity of photon emission time or location. This stochasticity results in a diffusion of the electron longitudinal coordinate even if the global phase slippage of the ring is zero, as we cannot make all the local or partial phase slippages zero simultaneously. As a consequence, there exists a lower bunch length limit and the energy spread grows significantly when the bunch length is pushed close to the limit. This bunch length limit and energy widening effect are first theoretically investigated by Shoji *et al.* [24,25] and recently more accurately analyzed by a part of

*dengxiujie@mail.tsinghua.edu.cn
†joerg.feikes@helmholtz-berlin.de
‡Roman.M.Klein@ptb.de
§markus.ries@helmholtz-berlin.de

Published by the American Physical Society under the terms of the Creative Commons Attribution 4.0 International license. Further distribution of this work must maintain attribution to the author(s) and the published article's title, journal citation, and DOI.

us using the longitudinal Courant-Snyder formalism [9,26]. This quantum diffusion is of crucial importance for SSMB and other ideas invoking ultrashort electron bunches in storage rings. As fundamental as it is, nevertheless, there is still no experiment confirming this effect. In this paper, we report the first experimental evidence supporting the existence of this effect. The experiment was conducted at the Metrology Light Source (MLS) [27–29] of the Physikalisch-Technische Bundesanstalt in Berlin.

II. THEORETICAL ANALYSIS

Before the presentation of the experimental work, here we give a brief overview of the theoretical analysis of this effect presented in Ref. [9] to make this paper more self-contained. The particle state vector $\mathbf{X} = (x, x', y, y', z, \delta)^T$ in 6D phase space is used, where x, x', y, y', z and $\delta = \Delta E/E_0$ are the horizontal position, angle, vertical position, angle, longitudinal position, and relative energy deviation with respect to the reference particle, respectively, and ^{T} means transpose. The three eigenemittances ϵ_k of a particle beam, with $k = I, II, III$, are the positive eigenvalues of $i\mathbf{\Sigma}\mathbf{S}$, where i is the imaginary unit, $\mathbf{\Sigma} = \langle \mathbf{X}\mathbf{X}^T \rangle$ are the second moments of the beam, and

$$\mathbf{S} = \begin{pmatrix} 0 & 1 & 0 & 0 & 0 & 0 \\ -1 & 0 & 0 & 0 & 0 & 0 \\ 0 & 0 & 0 & 1 & 0 & 0 \\ 0 & 0 & -1 & 0 & 0 & 0 \\ 0 & 0 & 0 & 0 & 0 & 1 \\ 0 & 0 & 0 & 0 & -1 & 0 \end{pmatrix}. \quad (2)$$

The eigenemittances are invariants with respect to linear symplectic transportation of the beam. In an electron storage ring, the equilibrium state is a balance between quantum excitation and radiation damping. According to Chao's solution by linear matrices (SLIM) formalism [30], the equilibrium eigenemittances are given by

$$\epsilon_k = \frac{C_L \gamma^5}{c\alpha_k} \oint \frac{|\mathbf{E}_{k5}(s)|^2}{|\rho(s)|^3} ds, \quad (3)$$

and the second moments of the beam are

$$\mathbf{\Sigma}_{ij} = 2 \sum_{k=I,II,III} \epsilon_k \mathrm{Re}[\mathbf{E}_{ki}\mathbf{E}^*_{kj}], \quad (4)$$

where α_k is the damping constant of the three eigenmodes, $C_L = 55 r_e \hbar/(48\sqrt{3} m_e)$, with $\hbar$ the reduced Planck's constant, r_e the electron classical radius, Re[] means taking the real part of a complex number, * means complex conjugate, and $\mathbf{E}_k$ is eigenvector of the 6×6 symplectic one-turn map, satisfying the following normalization condition

$$\mathbf{E}_k^\dagger \mathbf{S} \mathbf{E}_k = \begin{cases} i, & k = I, II, III, \\ -i, & k = -I, -II, -III, \end{cases} \quad (5)$$

and $\mathbf{E}_k^\dagger \mathbf{S} \mathbf{E}_j = 0$ for $k \neq j$, in which † means complex conjugate transpose. $\mathbf{E}_{ki}$ is the ith component of the eigenvector $\mathbf{E}_k$.

In a planar uncoupled storage ring, the one-turn map and its eigenvectors can be parametrized using the Courant-Snyder functions [9,31]. In this case, the longitudinal emittance is then defined as

$$\epsilon_z \equiv \left\langle \frac{z_\parallel^2 + [\alpha_z z_\parallel + \beta_z \delta]^2}{2\beta_z} \right\rangle, \quad (6)$$

where $z_\parallel = z - D'_x x - D_x x'$, $D'_x = \frac{dD_x}{ds}$ is the horizontal dispersion angle and α_z, β_z, γ_z are the Courant-Snyder functions in the longitudinal dimension. In the equilibrium state, the longitudinal emittance is given by

$$\epsilon_z = \frac{55}{96\sqrt{3}} \frac{\alpha_F \lambda\!\!\!^{-}{}_e^2 \gamma^5}{\alpha_L} \oint \frac{\beta_z(s)}{|\rho(s)|^3} ds, \quad (7)$$

in which α_L is the longitudinal radiation damping constant and nominally $\alpha_L \approx U_0/E_0$ with U_0 the radiation energy loss of an electron per turn, $\alpha_F = \frac{1}{137}$ is the fine structure constant, $\lambda\!\!\!^{-}{}_e = \lambda_e/2\pi = 386$ fm is the reduced Compton wavelength of the electron. Therefore, it is the longitudinal beta function β_z at the bending magnets that matters in determining the equilibrium longitudinal emittance ϵ_z. A physical picture is given in Fig. 1 to help better understand this argument.

If there is only a single radiofrequency (rf) cavity placed at a dispersion-free location in the ring, then at a specific position s_j, the ring can be divided into three parts, with their longitudinal transfer matrices given by

$$\begin{aligned} \mathbf{T}(s_{\mathrm{rf}}, s_j) &= \begin{pmatrix} 1 & -\tilde{\eta}(s_{\mathrm{rf}}, s_j) C_0 \\ 0 & 1 \end{pmatrix}, \\ \mathbf{T}(s_{\mathrm{rf}}, s_{\mathrm{rf}}) &= \begin{pmatrix} 1 & 0 \\ h & 1 \end{pmatrix}, \\ \mathbf{T}(s_j, s_{\mathrm{rf}}) &= \begin{pmatrix} 1 & -\tilde{\eta}(s_j, s_{\mathrm{rf}}) C_0 \\ 0 & 1 \end{pmatrix}, \end{aligned} \quad (8)$$

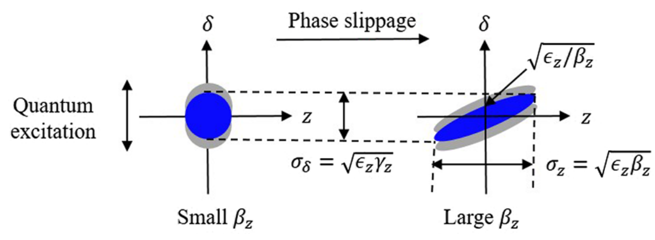

FIG. 1. A physical picture to explain why a larger longitudinal beta function β_z means a larger contribution to longitudinal emittance ϵ_z, with a given strength of quantum excitation.

where

$$\tilde{\eta}(s_2, s_1) = \frac{1}{C_0}\int_{s_1}^{s_2}\left(\frac{D_x(s)}{\rho(s)} - \frac{1}{\gamma^2}\right)ds \tag{9}$$

is the local or partial phase slippage from s_1 to s_2, and $\tilde{\eta}(s_{\rm rf}, s_j) + \tilde{\eta}(s_j, s_{\rm rf}) = \eta$, $h = eV_{\rm rf}k_{\rm rf}\cos\phi_s/E_0$ quantifies the rf acceleration gradient, in which e is the elementary charge, $V_{\rm rf}$ is the rf voltage, $k_{\rm rf} = 2\pi/\lambda_{\rm rf}$ is the rf wavenumber, and ϕ_s is the synchronous phase. In the analysis, the rf cavity is assumed to be a zero-length one. The one-turn map at s_j is then

$$\begin{aligned}\mathbf{M}(s_j) &= \mathbf{T}(s_j, s_{\rm rf})\mathbf{T}(s_{\rm rf}, s_{\rm rf})\mathbf{T}(s_{\rm rf}, s_j)\\ &= \begin{pmatrix} 1-\tilde{\eta}(s_j, s_{\rm rf})hC_0 & -\eta C_0 + \tilde{\eta}(s_j, s_{\rm rf})\tilde{\eta}(s_{\rm rf}, s_j)hC_0^2 \\ h & 1-\tilde{\eta}(s_{\rm rf}, s_j)hC_0\end{pmatrix}.\end{aligned} \tag{10}$$

A stable motion requires that

$$0 < h\eta C_0 < 4. \tag{11}$$

Following Courant and Snyder [31], we parametrize $\mathbf{M}(s_j)$ as

$$\mathbf{M}(s_j) = \begin{pmatrix} \cos\Phi_z + \alpha_z(s_j)\sin\Phi_z & \beta_z(s_j)\sin\Phi_z \\ -\gamma_z(s_j)\sin\Phi_z & \cos\Phi_z - \alpha_z(s_j)\sin\Phi_z\end{pmatrix}, \tag{12}$$

where $\Phi_z = 2\pi\nu_s$, $\nu_s = -\frac{\eta}{|\eta|}\frac{f_s}{f_0}$, f_s is the synchrotron oscillation frequency, and $f_0 = \frac{1}{T_0}$ is the revolution frequency of the particle in the ring. Therefore,

$$\beta_z(s_j) = \frac{\mathbf{M}_{12}(s_j)}{\sin\Phi_z} = \frac{-\eta C_0 + \tilde{\eta}(s_j, s_{\rm rf})\tilde{\eta}(s_{\rm rf}, s_j)hC_0^2}{\sin\Phi_z}, \tag{13}$$

Note that β_z is always positive, and

$$\begin{aligned}\frac{d\beta_z(s_j)}{ds_j} &= \frac{[\tilde{\eta}(s_{\rm rf}, s_j) - \tilde{\eta}(s_j, s_{\rm rf})]hC_0}{\sin\Phi_z}\left(\frac{D_x(s_j)}{\rho(s_j)} - \frac{1}{\gamma^2}\right)\\ &= 2\alpha_z(s_j)\left(\frac{D_x(s_j)}{\rho(s_j)} - \frac{1}{\gamma^2}\right),\end{aligned} \tag{14}$$

which is different from the conventional relation $\frac{d\beta_{x,y}}{ds} = -2\alpha_{x,y}$ in transverse dimensions [10].

The first term in the numerator of Eq. (13) is the conventional global phase slippage. The second term reflects the impact of the partial phase slippage on β_z. In usual rings, the second term is much smaller than the first term, therefore β_z is almost a constant value around the ring. The classical formulas of bunch length $\sigma_{z\rm S}$, energy spread $\sigma_{\delta\rm S}$, and longitudinal emittance $\epsilon_{z\rm S}$ are actually obtained with such approximation. Here in this paper, we use the subscript $_{\rm S}$ to represent the classical results obtained in the analysis of Sands [23]. More specifically, for an isomagnetic storage ring, we have

$$\begin{aligned}\beta_{z\rm S} &= \frac{-\eta C_0}{\sin\Phi_z} \approx \sqrt{\frac{\eta C_0}{h}},\\ \nu_s &= \frac{1}{2\pi}\arcsin\left(\frac{-\eta C_0}{\beta_{z\rm S}}\right) \approx -\frac{\eta}{|\eta|}\frac{\sqrt{h\eta C_0}}{2\pi},\\ \sigma_{z\rm S} &= \sqrt{\epsilon_{z\rm S}\beta_{z\rm S}} \approx \sqrt{\frac{C_q}{J_s}\frac{\gamma^2}{\rho}}\sqrt{\frac{\eta C_0}{h}} \approx \sigma_{\delta\rm S}\beta_{z\rm S},\\ \sigma_{\delta\rm S} &= \sqrt{\epsilon_{z\rm S}\gamma_{z\rm S}} \approx \sqrt{\frac{\epsilon_{z\rm S}}{\beta_{z\rm S}}} \approx \sqrt{\frac{C_q}{J_s}\frac{\gamma^2}{\rho}},\\ \epsilon_{z\rm S} &\approx \frac{C_q}{J_s}\frac{\gamma^2}{\rho}\sqrt{\frac{\eta C_0}{h}} \approx \sigma_{z\rm S}\sigma_{\delta\rm S} \approx \sigma_{\delta\rm S}^2\beta_{z\rm S},\end{aligned} \tag{15}$$

where $C_q = \frac{55\lambda\!\!\!^{-}_e}{32\sqrt{3}} = 3.8319 \times 10^{-13}$ m, J_s is the longitudinal damping partition number, and for a planar ring usually $J_s \approx 2$, ρ is the bending radius of the bending magnets. As can be seen, to generate short bunches in an electron storage ring, we need to implement a quasi-isochronous lattice, i.e., a small η, and a high rf gradient, i.e., a large h. We also note that the energy spread of an electron beam in the classical analysis is dominantly determined by the beam energy and bending radius of the bending magnets and has little dependence on the bunch length or global phase slippage of the ring.

Now with both terms in the numerator of Eq. (13) considered, the more accurate formula of the longitudinal emittance is then

$$\epsilon_z = \epsilon_{z\rm S}\left(1 + hC_0\frac{\langle\tilde{\eta}^2(s_j, s_{\rm rf})\rangle_\rho - \eta\langle\tilde{\eta}(s_j, s_{\rm rf})\rangle_\rho}{\eta}\right). \tag{16}$$

Note that $\langle\rangle_\rho$ here means the radiation-weighted average around the ring, defined as

$$\langle P\rangle_\rho = \frac{\oint\frac{P}{|\rho(s)|^3}ds}{\oint\frac{1}{|\rho(s)|^3}ds}, \tag{17}$$

i.e., the average is actually conducted at places with nonzero bending radius. After getting the longitudinal emittance and Courant-Snyder functions, the bunch length and energy spread at a specific location s_i are then

$$\begin{aligned}\sigma_z(s_i) &= \sqrt{\epsilon_z\beta_z(s_j)}\\ &\approx \sigma_{z\rm S}\sqrt{\frac{\epsilon_z}{\epsilon_{z\rm S}}}\sqrt{1 - \tilde{\eta}(s_i, s_{\rm rf})\tilde{\eta}(s_{\rm rf}, s_i)\frac{hC_0}{\eta}},\\ \sigma_\delta(s_i) &= \sqrt{\epsilon_z\gamma_z(s_i)} \approx \sigma_{\delta\rm S}\sqrt{\frac{\epsilon_z}{\epsilon_{z\rm S}}}.\end{aligned} \tag{18}$$

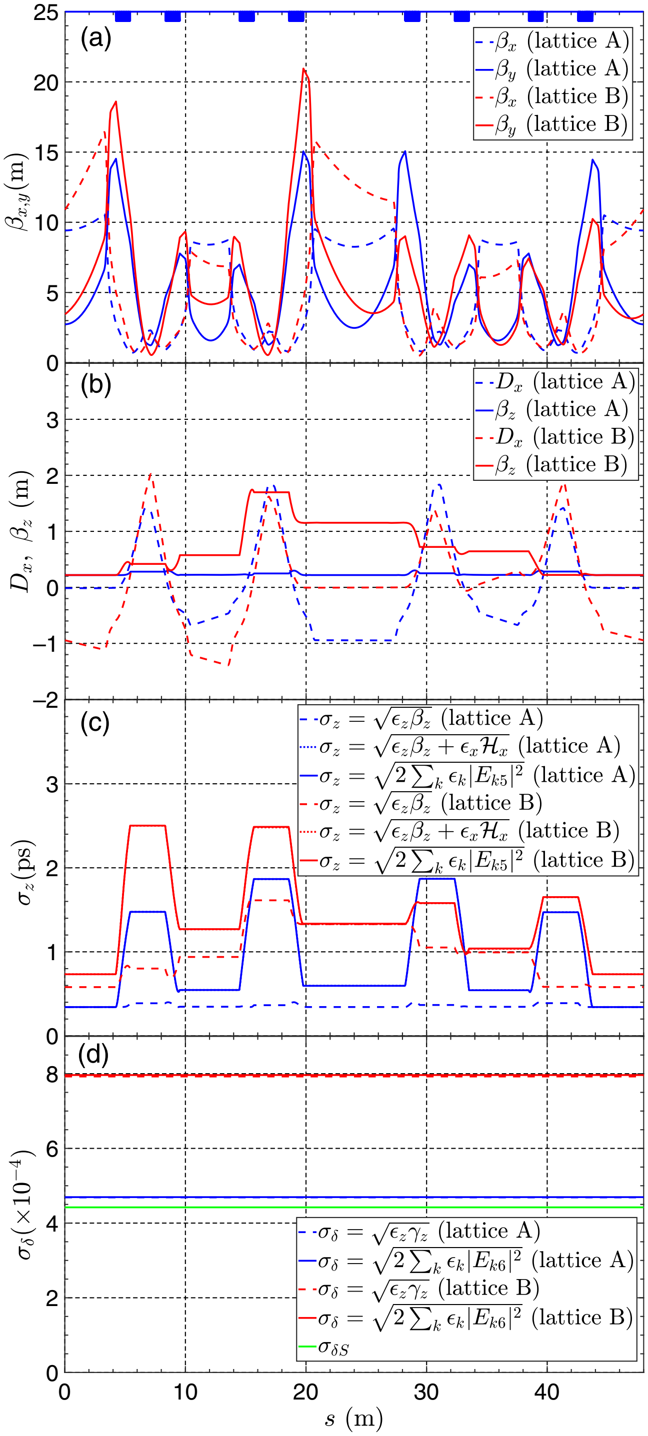

FIG. 2. Two lattices used in the experiment. Evolution of (a) $\beta_{x,y}$, (b) D_x and β_z, (c) σ_z, (d) σ_δ, around the ring. In this plot, the rf cavity is placed at $s_{\mathrm{rf}} = 0$ m, and $V_{\mathrm{rf}} = 600$ kV is applied, and the global phase slippage used is $\eta = 1 \times 10^{-5}$. The dipole magnets are shown at the top as blue rectangles. Each dipole has a length of 1.2 m and bends the electron trajectory for an angle of $\pi/4$. $\beta_{x,y}$ and D_x are obtained by fitting a model to the BPM-corrector response matrix (LOCO) [32]. The bunch length and energy spread evolution are calculated based on the longitudinal Courant-Snyder formalism and SLIM formalism.

We remind the readers that the energy spread and γ_z are unchanged outside the rf cavity. In addition, if the contribution of $\frac{1}{\gamma^2}$ is negligible in the definition of η, α_z, and β_z will vary notably only inside the bending magnets. Actually, the chromatic $\mathcal{H}_x$ function, a parameter quantifying the coupling of horizontal emittance to bunch length as will be given in Eq. (21), also changes only inside the bending magnets. Both arguments reveal the fact that in ultrarelativistic cases, bunch length changes only inside the bending magnets. We will see this clearly in Fig. 2.

By investigating the bunch length at the rf cavity

$$\sigma_z(s_{\mathrm{rf}}) \approx \sigma_{z\mathrm{S}}\sqrt{\frac{\epsilon_z}{\epsilon_{z\mathrm{S}}}} = \sigma_{\delta\mathrm{S}}\sqrt{\frac{\eta}{hC_0} + \langle\tilde{\eta}^2(s_j, s_{\mathrm{rf}})\rangle_\rho - \eta\langle\tilde{\eta}(s_j, s_{\mathrm{rf}})\rangle_\rho C_0}, \quad (19)$$

we observe that there exists a lower bunch length limit when η approaches zero

$$\sigma_{z,\mathrm{limit}} = \sigma_{\delta\mathrm{S}}\sqrt{\langle\tilde{\eta}^2(s_j, s_{\mathrm{rf}})\rangle_\rho C_0}. \quad (20)$$

This limit is the main consequence of the unavoidable quantum diffusion of longitudinal coordinates in a storage ring. It has little dependence on the global phase slippage and rf voltage, once the beam energy and dispersion function pattern around the ring is given. Since $\sigma_{z\mathrm{S}} \propto \sqrt{|\eta|}$, the above bunch length limit means $\frac{\epsilon_z}{\epsilon_{z\mathrm{S}}}$ will diverge as η approaches zero. The energy spread will thus diverge in this process.

While the bunch length at the rf cavity will saturate at the limit given by Eq. (20) with the decrease of η, the bunch length at other places, from which the partial phase slippage to the rf cavity is large, may first decrease and then increase. The reason is that the increased energy spread will lead to bunch lengthening through the partial phase slippage from the rf cavity to the specific location. In other words, the longitudinal beta function ratio between that at the rf cavity and that at the specific location may increase with the lowering of η.

III. EXPERIMENTAL VERIFICATION

Now, we present our experimental work on this quantum diffusion effect. For usual rings, the bunch length limit given by Eq. (20) is a couple of 10 fs to about 100 fs, while the typical bunch length in operation is at 10 ps level. So this effect is negligible in almost all existing rings. However, with the accelerator physics and technologies continuing to advance, more ambitious goals of bunch length can be envisioned and realized in the future to benefit more from the electron beam. For example, in an SSMB storage ring, the desired bunch length is submicron or even nanometer, which corresponds to sub-fs in unit of time. The quantum diffusion investigated here then becomes the first fundamental issue that needs to be resolved. With such motivation to develop an SSMB light source, and considering that it is a fundamental physical effect by itself, we believe it is important to experimentally verify this effect.

To observe the influence of this effect, we need the second term in the bracket of Eq. (16) to be comparable or larger than 1, which is nontrivial for many of the existing storage rings. Other collective and single-particle effects stand in the way before arriving at such a small value of η. However, because of the dedicated quasi-isochronous lattice design and the individually independent magnet power supplies of the MLS storage ring, there is great flexibility in tailoring the lattice optics to obtain a locally large and globally small phase slippage simultaneously, thus opening the possibility to see this effect in an existing machine. Another characteristic making the MLS an ideal test bed for single-particle beam dynamical effects is that it can operate with a beam current ranging from 1 pA (a single electron) to 200 mA.

We have prepared two quasi-isochronous lattice optics at the MLS, named lattice A and B, respectively. Lattice A is the standard quasi-isochronous lattice, whereas lattice B is developed and dedicated to this experiment. The optical functions of the two lattices are shown in Fig. 2. Other related parameters of the two lattices are given in Table I. The key difference between these two lattices is that lattice B has a much larger local phase slippage and average value of β_z. Therefore, the bunch length limit of lattice B (469 fs at 630 MeV) due to this quantum diffusion is larger than that in lattice A (115 fs at 630 MeV). Note that with the given parameters set, β_z in lattice A is almost a constant value around the ring, while β_z in lattice B varies significantly and in many places is much larger than that in lattice A.

TABLE I. Parameters of the two lattices of the MLS storage ring used in the experiment.

Parameter	Value	Description
C_0	48 m	Ring circumference
E_0	630 MeV	Beam energy
U_0	9.14 keV	Radiation energy loss
f_{rf}	500 MHz	rf frequency
V_{rf}	600 kV	rf voltage
h_{rf}	0.01 m^{-1}	rf acceleration gradient
$\sigma_{\delta\mathrm{S}}$	4.4×10^{-4}	Classical energy spread
ϵ_x	197.3 nm	Lattice A
J_s	1.95	Lattice A
$\langle\tilde{\eta}(s_j,s_{\mathrm{rf}})\rangle_\rho$	2.5×10^{-5}	Lattice A
$\sqrt{\langle\tilde{\eta}^2(s_j,s_{\mathrm{rf}})\rangle_\rho}$	1.6×10^{-3}	Lattice A
$\sigma_{z,\mathrm{limit}}$	34 μm (115 fs)	Lattice A
ϵ_x	219.4 nm	Lattice B
J_s	1.95	Lattice B
$\langle\tilde{\eta}(s_j,s_{\mathrm{rf}})\rangle_\rho$	-5.5×10^{-3}	Lattice B
$\sqrt{\langle\tilde{\eta}^2(s_j,s_{\mathrm{rf}})\rangle_\rho}$	6.7×10^{-3}	Lattice B
$\sigma_{z,\mathrm{limit}}$	142 μm (469 fs)	Lattice B

As can be seen in Fig. 2, the magnitudes of horizontal dispersion function D_x of lattice B are large at some of the bending magnets, which according to Eq. (9) means the local phase slippage increases or decreases sharply within them, leading to a large variation of local phase slippage $\tilde{\eta}$ and β_z. The small global phase slippage η is realized by canceling the contribution of positive and negative D_x at different bending magnets. We remind the readers that this lattice can also be used for the delayed alpha buckets study in which the momentum differences of particles in different alpha buckets can be translated into large arrival time differences through the large partial phase slippage [29], which might be useful for some user experiments.

To evaluate the possibility of verifying this effect experimentally, the bunch length and energy spread evolution around the ring in these two lattices have also been presented in Fig. 2. Note that the bunch length formula in Eq. (18) contains only the contribution from longitudinal emittance. Considering the bunch lengthening by horizontal emittance at dispersive locations, the more accurate formula of bunch length is [8,33]

$$\sigma_z = \sqrt{\epsilon_z\beta_z + \epsilon_x\mathcal{H}_x}, \tag{21}$$

with $\mathcal{H}_x = \gamma_x D_x^2 + 2\alpha_x D_x D_x' + \beta_x D_x'^2$ being the horizontal chromatic function. Strictly speaking, Courant-Snyder and dispersion functions are only well defined in a planar uncoupled lattice and only when the rf cavity is placed at a dispersion-free location. For a general coupled lattice, the more accurate SLIM formalism should be referred, i.e.,

$$\sigma_z = \sqrt{2\sum_{k=I,II,III}\epsilon_k|\mathbf{E}_{k5}|^2},$$
$$\sigma_\delta = \sqrt{2\sum_{k=I,II,III}\epsilon_k|\mathbf{E}_{k6}|^2}. \tag{22}$$

On the other hand, although the rf cavity is placed at a dispersive location in lattice B, we have confirmed that the Courant-Snyder parametrization for beam dynamics analysis, in this case, is still largely valid since the difference of result between that given by longitudinal Courant-Snyder formalism and the more accurate SLIM formalism is very small.

As can be seen in Fig. 2, in which the global phase slippage η is lowered to be 1×10^{-5}, which corresponds to a synchrotron frequency of $f_s = 2.2$ kHz with $V_{\mathrm{rf}} = 600$ kV, the energy spread grows to be $\sigma_\delta = 7.9\times10^{-4}$, while the classical energy spread is $\sigma_{\delta\mathrm{S}} = 4.4\times10^{-4}$.

Such an amount of energy spread growth is detectable by measuring the spectra of Compton-backscattered (CBS) photons from the head-on collision between a CO_2 laser with the electron beam at the MLS [27,34]. In addition, the bunch length difference in these two lattices is large enough to be observable by investigating the spectra and power of coherent THz radiation and invoking streak camera measurement.

To exclude the influence of collective effects, the beam current is lowered to around 6 μA/bunch in a multibunch filling mode in the experiment. There is no indication of microwave or other collective instabilities. The beam is stable (no fluctuation of radiation source point observed) and its width and energy spread are independent of the beam current when the single-bunch current is as low as the value applied in the experiment. The horizontal chromaticity has been carefully corrected close to zero (about 0.05) to minimize the beam energy widening arising from the betatron motion of particles reported in our previous work [7]. The longitudinal chromaticity has also been corrected to a small value to mitigate longitudinal nonlinear dynamics. We note that a large quantum diffusion of longitudinal coordinate (a root-mean-square value of 0.54 μm or 1.8 fs per turn in lattice B at 630 MeV) actually helps suppress collective beam instability of ultrahigh frequency, as it will disperse any fine time structure in an electron beam like density modulation and energy modulation [25].

To get an idea about the bunch length in the two lattices, first, we measure the coherent THz radiation spectra and power as a function of the synchrotron tune in the two lattices. The shorter the electron bunch, the higher frequency range the coherent THz radiation spectra extend and the larger radiation power we can obtain. In the experiment, the synchrotron frequency ($f_s \propto \sqrt{|\eta|}$), thus the global phase slippage η, is controlled by slightly changing the quadrupole currents while keeping the dispersion function pattern unchanged. The THz beamline has its source point at $\frac{\pi}{16}$ bending angle ($s = 38.775$ m) at the seventh dipole, counted from $s = 0$ m in Fig. 2 which is where the rf cavity is placed. For getting the coherent synchrotron radiation emission spectra in the THz spectral range, a commercial, Michelson-type FTIR spectrometer (Vertex 80v) in combination with a 4K liquid helium-cooled composite silicon bolometer was used for measuring interferograms. After fast Fourier transform of the data, the emitted spectrum can directly be accessed. For this experiment, a series of 128 interferograms has been acquired and the average Fourier transformed.

The measured coherent THz radiation power, integrated with wave number from 1 to 20 cm^{-1}, together with the theoretical bunch length at the THz observation calculated using Eq. (21) are shown in Fig. 3(a). The measurement results agree with our expectations reasonably well. In particular, we notice that in lattice B, the THz power first increases and then decreases, with the lowering of the synchrotron tune, while the radiation power in lattice A monotonically decreases and then saturates in this process. This observation agrees well with our theoretical prediction of the bunch length evolution in these two lattices. Not presented here, we also notice that the frequency range of the spectra evolves consistently with the integrated power, i.e., a larger THz power corresponds to a higher frequency range coverage. To be more rigorous, we remind the readers that the bunch length in lattice A at the THz radiation observation point in principle will also diverge, as explained in the last section, if we push the phase slippage factor of the ring even closer to zero, which in practice is a demanding work.

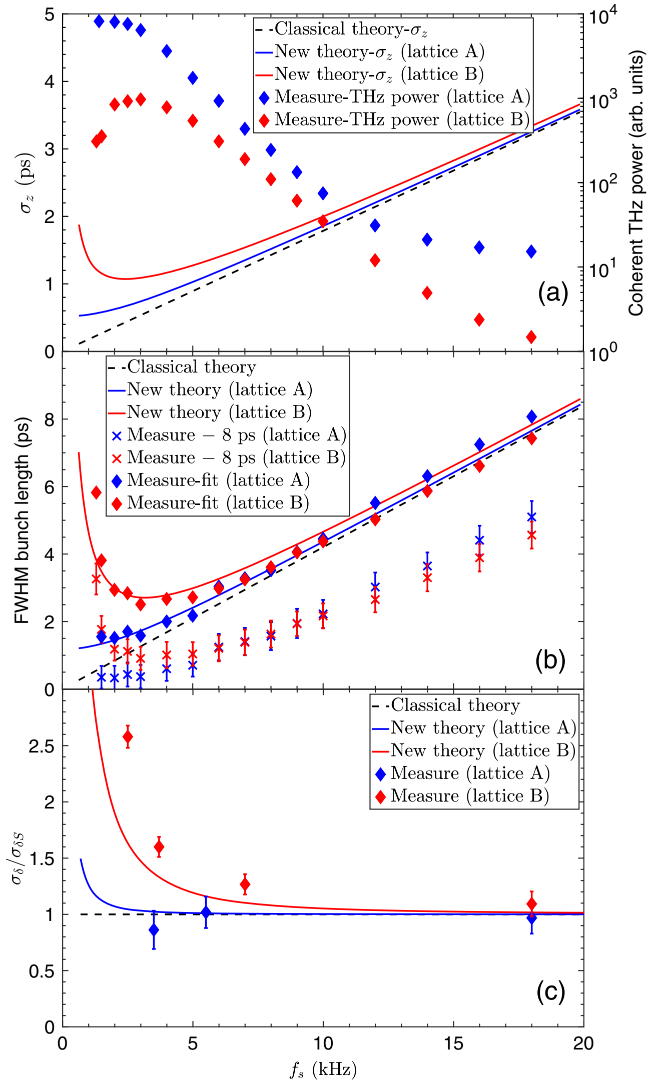

FIG. 3. Experiment measurement results and comparison with theory. (a) Theoretical bunch length and measured coherent THz radiation power observed at $s = 38.775$ m, in lattice A and B, respectively. (b) Theoretical, measured raw data (shifted 8 ps downwards) and fitted bunch length at $s = 24$ m, in lattice A and B, respectively. (c) Theoretical and measured electron beam energy spreads σ_δ normalized by the classical energy spread $\sigma_{\delta S}$ vs the synchrotron frequency f_s, in lattice A and B, respectively.

During the measurement of coherent THz radiation, we at the same time employed a streak camera to measure the electron bunch length directly. The streak camera at the MLS is installed at the undulator beamline (opposite the rf cavity, $s = 24$ m in Fig. 2). For the experiment, the undulator was closed from the "open" gap of 180 mm to 45.7 mm to have the first harmonic undulator radiation at a visible wavelength available for the streak camera. The measurement results of bunch length and the comparison with theory is presented in Fig. 3(b). Note that we have shifted the measured raw data downwards by 8 ps in the plot. The error bars in the plot are the standard deviation of the fitted results for each single column of the recorded streak camera image. Again, we observe the significant difference in the two lattices concerning the bunch length evolution as a function of the synchrotron tune, which agrees qualitatively with the theory. However, quantitatively, the measured raw data of bunch length deviate notably from the theoretic prediction.

Realizing that there will be unavoidable systematic errors concerning the streak camera measurement because we are close to its resolution limit, we try to use the model below to fit the data with the theory,

$$\Delta z_{\mathrm{fit}} = \sqrt{\Delta z_{\mathrm{measure}}^2 - \mathrm{noise}^2} - \mathrm{offset}, \tag{23}$$

where Δz means the bunch length. Note that here we use the full width at half maximum (FWHM), instead of the root mean square, to quantify the bunch length, since in the real case, the bunch profile is unavoidable non-Gaussian to some extent, especially when the phase slippage factor of the ring is small. The noise in the above equation is used to model the square sum-type error, while the offset accounts for the systematic shift concerning the measurement results. The fitted data (noise = 7 ps and offset = 3 ps applied) agrees well with the theoretical curve as shown in Fig. 3(b). We remind the readers that all the data points in the plot are modeled with the same noise and offset.

Further, we have measured the electron beam energy spread in the two lattices, using the head-on CBS between a CO_2 laser with the electron beam. Note that the rf voltage applied in the above bunch length measurements is 500 kV, while now it is 600 kV when doing the energy spread measurement. The measurement of CBS photon spectra and the evaluation of electron beam energy spread based on it is a well-established method implemented at the MLS and is used in this experiment to confirm the energy widening as we push the bunch length close to the limit, by lowering the global phase slippage η. More details about this CBS method can be found in Refs. [27,34]. Quantitative analysis revealing the energy spreads σ_δ normalized by the classical energy spread $\sigma_{\delta S}$, and its comparison with the theoretical prediction from Eq. (18) for two different lattices are shown in Fig. 3(c). The error bars in Fig. 3(c) are the root-mean-square uncertainties of the measurements and are due to calibration errors and counting statistics. The data acquisition time of a photon spectrum is 15 min. It can be seen from Fig. 3 that in lattice B, the energy spread grows significantly with the decrease of η, in the figure synchrotron frequency f_s, to the level of 1×10^{-5}, while the energy spread stays almost constant in lattice A. Again the measurement agrees qualitatively with the theory.

There is still some deviation of the measured energy widening and the theoretical prediction for lattice B. Candidate explanations are as follows: first, there is some uncertainty in the determination of synchrotron frequency f_s, especially when f_s is lowered to 2–3 kHz, considering the fact that the peak of the synchrotron frequency spectrum then can be as wide as 0.5 kHz; second, there could be some remaining higher-order phase slippages that may contribute to the energy spread growth when η is small due to its impact on the longitudinal phase space bucket, while the theory assumes a linear phase slippage.

The above-presented measurements of bunch length and energy spread are very demanding and are moving on the edge of the experimentally accessible parameter space. Nevertheless, we see a nice qualitative agreement with the theory presented in the first part of this paper, proofing important experimental evidence to support the theoretical analysis. As far as we know, this type of investigation can actually not be performed at any other operating storage ring. However, we recognize that the deviation of the quantitative numbers between the measurements and theory concerning both the bunch length and energy spread emphasizes the need for an even more improved model. Summarizing, we state that our experimental work supports the existence of the analyzed quantum diffusion effect and the argument that the quantum excitation on longitudinal emittance at a given location depends on the longitudinal beta function there. The evidence, however, is not strong enough to claim this is fully consistent proof of the effect.

IV. DISCUSSIONS

The existence of this quantum diffusion means the classical formulas of bunch length and energy spread break down in a ring with ultrasmall global and large local phase slippage. To realize an ultrashort bunch length and ultrasmall longitudinal emittance in an electron storage ring, both the global and local phase slippages should be well confined to minimize β_z at all the bending magnets. Based on the presented longitudinal Courant-Snyder formalism, we can derive the scaling of the theoretical minimum bunch length and longitudinal emittance in a longitudinal weak focusing ring ($\nu_s \ll 1$) with respect to the bending radius ρ and angle θ of each bending magnet [20]

$$\sigma_{z,\min} \approx \frac{\sqrt{2415}}{20160}\sqrt{\frac{C_q}{J_s}}\sqrt{\rho}\gamma\theta^3 \propto \sqrt{\rho}\gamma\theta^3,$$
$$\epsilon_{z,\min} \approx 2\frac{\sqrt{2415}}{20160}\frac{C_q}{J_s}\gamma^2\theta^3 \propto \gamma^2\theta^3. \tag{24}$$

A comprehensive analysis of longitudinal emittance minimization in an electron storage ring can be found in Ref. [10]. Now we can do some evaluation based on Eq. (24). For example, if we want to realize steady-state microbunches with a bunch length of 10 nm in a storage ring at $E_0 = 400$ MeV, then we need $\sigma_{z,\min} < 10$ nm to make sure the energy spread will not grow much when the bunch length is pushed to the desired 10 nm. If $\rho = 2$ m, then we need $\theta \lesssim \frac{\pi}{17}$ (corresponding to $\sigma_{z,\min} = 7.5$ nm and $\epsilon_{z,\min} = 3.6$ pm), which means we need around 34 bending magnets in total for the ring. Assuming that the length of each quasi-isochronous cell containing a bending magnet (length of $\rho\theta = 0.37$ m) is about 2 m, then the arc section of the ring is about 68 m in length. Considering the space needed for laser modulator which is the bunching system for SSMB, radiation generation section, the energy replenish system, etc., the circumference of such an SSMB storage ring can be 80 to 100 m.

According to Eq. (24), in principle, we can always implement a smaller bending angle for each bending magnet when we want a smaller bunch length. However, if the desired bunch length is as short as the nm level, the required global phase slippage will be too small in practice. On the other hand, we remind the readers that the bunch length limit given in Eq. (24) is derived assuming that the ring is working in the longitudinal weak focusing regime. If we want to obtain a bunch length even shorter, longitudinal strong focusing can be envisioned not unlike its transverse counterpart [35,36] which is the basis for modern particle accelerators. This approach of getting extremely short bunches in SSMB is called longitudinal strong focusing SSMB [3,9,21]. Another possible way of realizing ultrashort bunches is by invoking a transverse-longitudinal coupled lattice since then there will be some freedom in projecting the three eigenemittances of the electron beam into different physical dimensions. By taking advantage of the fact that the vertical emittance in a planar electron storage ring is rather small, the application of such transverse-longitudinal coupling schemes can help relax the requirement on the modulation laser power to realize extremely short electron bunches in SSMB [11,37]. Such a turn-by-turn transverse-longitudinal coupling-based bunch compression scheme can be viewed as a generalized longitudinal strong focusing [18,20].

ACKNOWLEDGMENTS

This work is supported by the National Key Research and Development Program of China (Grant No. 2022YFA1603401) and the National Natural Science Foundation of China (NSFC Grant No. 12035010). The work of Deng is supported by Shuimu Tsinghua Scholar Program of Tsinghua University.

[1] D. F. Ratner and A. W. Chao, Steady-State Microbunching in a Storage Ring for Generating Coherent Radiation, Phys. Rev. Lett. **105**, 154801 (2010).

[2] Y. Jiao, D. F. Ratner, and A. W. Chao, Terahertz coherent radiation from steady-state microbunching in storage rings with X-band radio-frequency system, Phys. Rev. ST Accel. Beams **14**, 110702 (2011).

[3] A. Chao, E. Granados, X. Huang, D. Ratner, and H.-W. Luo, High power radiation sources using the steady-state microbunching mechanism, in *Proceedings of the 7th International Particle Accelerator Conference, IPAC-16, Busan, Korea, 2016* (JACoW, Geneva, Switzerland, 2016), pp. 1048–1053.

[4] S. Khan, Ultrashort high-brightness pulses from storage rings, Nucl. Instrum. Methods Phys. Res., Sect. A **865**, 95 (2017).

[5] C. Tang, X. Deng, A. Chao, W. Huang, T. Rui, J. Feikes, J. Li, M. Ries, A. Hoehl, D. Ratner *et al.*, An overview of the progress on SSMB, in *Proceedings of the 60th ICFA Advanced Beam Dynamics Workshop on Future Light Sources, FLS'18, Shanghai, China, 2018* (JACoW, Geneva, Switzerland, 2018), pp. 166–170.

[6] Z. Pan, T. Rui, W. Wan, A. Chao, X. Deng, Y. Zhang, W. Huang, and C. Tang, A storage ring design for steady-state microbunching to generate coherent EUV light source, in *Proceedings of the 39th International Free Electron Laser Conference, FEL'19, Hamburg, Germany, 2019* (JACoW, Geneva, Switzerland, 2019), pp. 700–703.

[7] X. J. Deng, R. Klein, A. W. Chao, A. Hoehl, W. H. Huang, J. Li, J. Lubeck, Y. Petenev, M. Ries, I. Seiler, C. X. Tang, and J. Feikes, Widening and distortion of the particle energy distribution by chromaticity in quasi-isochronous rings, Phys. Rev. Accel. Beams **23**, 044001 (2020).

[8] X. J. Deng, A. W. Chao, J. Feikes, W. H. Huang, M. Ries, and C. X. Tang, Single-particle dynamics of microbunching, Phys. Rev. Accel. Beams **23**, 044002 (2020).

[9] X. J. Deng, A. W. Chao, W. H. Huang, and C. X. Tang, Courant-Snyder formalism of longitudinal dynamics, Phys. Rev. Accel. Beams **24**, 094001 (2021).

[10] Y. Zhang, X. J. Deng, Z. L. Pan, Z. Z. Li, K. S. Zhou, W. H. Huang, R. K. Li, C. X. Tang, and A. W. Chao, Ultralow longitudinal emittance storage rings, Phys. Rev. Accel. Beams **24**, 090701 (2021).

[11] X. Deng, W. Huang, Z. Li, and C. Tang, Harmonic generation and bunch compression based on transverse-longitudinal coupling, Nucl. Instrum. Methods Phys. Res., Sect. A **1019**, 165859 (2021).

[12] C.-Y. Tsai, A. W. Chao, Y. Jiao, H.-W. Luo, M. Ying, and Q. Zhou, Coherent-radiation-induced longitudinal single-pass beam breakup instability of a steady-state microbunch train in an undulator, Phys. Rev. Accel. Beams **24**, 114401 (2021).

[13] C.-Y. Tsai, Theoretical formulation of multiturn collective dynamics in a laser cavity modulator with comparison to Robinson and high-gain free-electron laser instability, Phys. Rev. Accel. Beams **25**, 064401 (2022).
[14] C. Tang and X. Deng, Steady-state micro-bunching accelerator light source, Acta Phys. Sin. **71**, 152901 (2022).
[15] Y. Lu, X. Wang, X. Deng, C. Feng, and D. Wang, Methods for enhancing the steady-state microbunching in storage rings, Results Phys. **40**, 105849 (2022).
[16] X. J. Deng, Y. Zhang, Z. L. Pan, Z. Z. Li, J. H. Bian, C.-Y. Tsai, R. K. Li, A. W. Chao, W. H. Huang, and C. X. Tang, Average and statistical properties of coherent radiation from steady-state microbunching, J. Synchrotron Radiat. **30**, 35 (2023).
[17] T. Li, Z. Liu, X. Deng, L. Yan, and C. Tang, A Fokker-Planck analysis of laser phase noise in a steady-state microbunching storage ring, Front. Phys. (to be published).
[18] Z. Li, X. Deng, Z. Pan, C. Tang, and A. Chao, A Generalized Longitudinal Strong Focusing Storage Ring, Phys. Rev. Lett. (to be published); Generalized longitudinal strong focusing in a steady-state microbunching storage ring, Phys. Rev. Accel. Beams (to be published).
[19] Z. Pan, Research on optimization and design of Advanced Laser-driving Storage Ring, Ph.D. thesis, Tsinghua University, Beijing, China, 2020.
[20] X. Deng, Theoretical and experimental studies on steady-state microbunching, Ph.D. thesis, Tsinghua University, Beijing, China, 2022.
[21] Y. Zhang, Research on longitudinal strong focusing SSMB ring, Ph.D. thesis, Tsinghua University, Beijing, China, 2022.
[22] X. Deng, A. Chao, J. Feikes, A. Hoehl, W. Huang, R. Klein, A. Kruschinski, J. Li, A. Matveenko, Y. Petenev *et al.*, Experimental demonstration of the mechanism of steady-state microbunching, Nature (London) **590**, 576 (2021).
[23] M. Sands, The physics of electron storage rings: An introduction, SLAC Technical Report No. SLAC-121, 1970.
[24] Y. Shoji, H. Tanaka, M. Takao, and K. Soutome, Longitudinal radiation excitation in an electron storage ring, Phys. Rev. E **54**, R4556 (1996).
[25] K. Soutome, M. Takao, H. Tanaka, and Y. Shoji, Longitudinal radiation excitation of quasi-isochronus storage ring “New SUBARU”, in *Proceedings of the 6th European Particle Accelerator Conference EPAC’98, Stockholm, Sweden, 1998* (Institute of Physics Publishing, Bristol and Philadelphia, 1998), pp. 1008–1010.
[26] C. Biscari, Bunch length modulation in highly dispersive storage rings, Phys. Rev. ST Accel. Beams **8**, 091001 (2005).
[27] R. Klein, G. Brandt, R. Fliegauf, A. Hoehl, R. Müller, R. Thornagel, G. Ulm, M. Abo-Bakr, J. Feikes, M. v. Hartrott, K. Holldack, and G. Wüstefeld, Operation of the Metrology Light Source as a primary radiation source standard, Phys. Rev. ST Accel. Beams **11**, 110701 (2008).
[28] J. Feikes, M. von Hartrott, M. Ries, P. Schmid, G. Wüstefeld, A. Hoehl, R. Klein, R. Müller, and G. Ulm, Metrology Light Source: The first electron storage ring optimized for generating coherent THz radiation, Phys. Rev. ST Accel. Beams **14**, 030705 (2011).
[29] M. Ries, Nonlinear momentum compaction and coherent synchrotron radiation at the Metrology Light Source, Ph.D. dissertation, Humboldt University of Berlin, Berlin, Germany, 2014).
[30] A. W. Chao, Evaluation of beam distribution parameters in an electron storage ring, J. Appl. Phys. **50**, 595 (1979).
[31] E. D. Courant and H. S. Snyder, Theory of the alternating-gradient synchrotron, Ann. Phys. (N.Y.) **3**, 1 (1958).
[32] J. Safranek, Experimental determination of storage ring optics using orbit response measurements, Nucl. Instrum. Methods Phys. Res., Sect. A **388**, 27 (1997).
[33] Y. Shoji, Bunch lengthening by a betatron motion in quasi-isochronous storage rings, Phys. Rev. ST Accel. Beams **7**, 090703 (2004).
[34] R. Klein, T. Mayer, P. Kuske, R. Thornagel, and G. Ulm, Beam diagnostics at the BESSY I electron storage ring with Compton backscattered laser photons: measurement of the electron energy and related quantities, Nucl. Instrum. Methods Phys. Res., Sect. A **384**, 293 (1997).
[35] N. Christofilos, Focusing system for ions and electrons, U.S. Patent No. 2,736,799 (1950).
[36] E. D. Courant, M. S. Livingston, and H. S. Snyder, The strong-focusing synchroton—A new high energy accelerator, Phys. Rev. **88**, 1190 (1952).
[37] C. Feng and Z. Zhao, A storage ring based free-electron laser for generating ultrashort coherent EUV and x-ray radiation, Sci. Rep. **7**, 4724 (2017).